International Flame Research Foundation
The Finnish and Swedish National Committees
Finnish – Swedish Flame Days 2013

TIME-AVERAGED SIMULATION OF THE FURNACE OF A CHINESE 135MWe CFB BOILER

Juho Peltola*, Sirpa Kallio

VTT Technical Research Centre of Finland
Metallimiehenkuja 6, Espoo; P.O.Box 1000; FI-02044 VTT, Finland

* Corresponding author, juho.peltola@vtt.fi

ABSTRACT

Several alternative methods for simulation of circulating fluidized beds (CFB) have been suggested. Transient simulations require either a small time step, a fine mesh and an unfeasibly long simulation time or rigorous closure models that account for the mesh spacing. To reduce computing time, steady-state 3D models have been suggested especially for simulation of industrial CFBs. In Taivassalo et al. (2011), a time-averaged simulation approach for a CFB was introduced and later the approach, combined with a Lagrangian particle tracking of fuel particles, was applied on CFB combustion in a 12 MW boiler. In Peltola et al. (2013), a similar approach was applied to 120 MWe load conditions in a commercial 135 MWe CFB boiler located in Ruzhou, China.

In the present study, two cases at different loads in the Chinese boiler are simulated and the results are compared to assess the capability of the time-averaged models to respond to changes in process conditions. The simulation results show a typical voidage distribution in a CFB. Gas composition profiles show reasonable distributions of oxygen and combustion products inside the furnace. The difference between the two operational modes is at least qualitatively reproduced.

Keywords: CFB; CFD modeling; combustion

1 Introduction

Circulating fluidized bed (CFB) combustion can be simulated in 3D with several alternative approaches. The transient Eulerian-Eulerian method based on the kinetic theory of granular flow that treats solids as a continuous phase is commonly used for simulation of hydrodynamics in small scale CFBs. It is available in CFD codes like Ansys Fluent, OpenFOAM, and MFiX. With either Eulerian or Lagrangian (particle tracking) description of the fuel, it can be applied to CFB combustion. Large fluctuations in the flow and a wide range of length and time scales are typical for a CFB. To adequately resolve the structures in a transient simulation a fine computational mesh is required. In practice, however, restrictions on computation time make it

necessary to use a coarse computational mesh that filters out the fine structures. Thus mesh spacing dependent subgrid closures should be applied to obtain realistic results. Some closures have been suggested and applied in the literature but so far no general models are available. The transient Eulerian-Eulerian method, together with special coarse mesh closures for gas-particle drag force, is mainly used for small furnaces (e.g. Nikolopoulos (2010)) or in 2D but also for industrial boilers (e.g. Zhang et al. (2010)).

Lagrangian particle tracking, used in small scale simulations, is not feasible in large geometries in dense suspension conditions that are dominated by particle-particle interactions. They cannot thus be used for CFB boilers. An approach, available e.g. in Ansys Fluent and Barracuda CFD codes, that combines Lagrangian and Eulerian solids description is the transient multiphase particle-in-cell (MP-PIC) method (Andrews & O'Rourke (2011)), which tracks parcels of particles and thus allows an easy description of particle size distributions. For practical reasons, a coarse mesh is a necessity even in this case and thus the method suffers from similar, so far unresolved, mesh-spacing related problems (Benyahia & Sundaresan (2012)) as the transient Eulerian-Eulerian methods.

All the above methods are based on transient simulations and require time-averaging over a long simulation time, which renders the computations slow. Consequently, there are obvious benefits in solving the flow at steady state. Furthermore, at steady state the fine structures of the transient simulations disappear and a fairly coarse mesh suffices to produce acceptable space resolution.

For fast simulation, macroscopic steady state models have been developed (Pallarès & Johnsson (2006)) based on simplified empirical descriptions of material distribution and transport phenomena. The benefits of these methods are robustness and speed, but as a drawback, a significant amount of empirical correlations is required.

Another alternative that allows fast steady state simulation of CFBs is time-averaged CFD modeling based on equations derived by averaging the transient Eulerian-Eulerian equations over time. The level of abstraction and need for closures is similar to what is required in macroscopic models, but since the transport equations are based on averaging the corresponding transient equations, the model should react to changes in the process conditions in a more natural way. Taivassalo & al. (2011) introduced a time-averaged CFD model and in Taivassalo & al. (2012), the approach was applied on CFB combustion in Chalmers 12 MW boiler. In addition to hydrodynamics, models for heat transfer and chemistry were included in the model. The behavior of fuel particles was simulated with a Lagrangian approach.

In Peltola et al. (2013), a steady state simulation approach was applied to a situation with uneven lateral fuel distribution at 120 MWe load in a commercial 135 MWe CFB boiler located in Ruzhou, China. In the present study, two conditions in the boiler are simulated with somewhat modified closures and the results are compared to assess the capability of the time-averaged models to respond to changes in process conditions.

2 Case description

The 135 MWe CFB boiler and the measurement arrangements are described in Peltola et al. (2013). The simulated region is shown in Figure 1. The conical bottom section is

refractory lined while other walls are membrane covered. Six hanging super heaters and four re-heaters are located in the upper part of the furnace.

A membrane wall in the middle of the furnace to a large extent splits the furnace in two sections to allow flexible furnace operation. Coal is fed through six coal feeders on the front wall. Secondary air enters from two levels at the front and back walls and some additional air comes from four ash coolers at the furnace sides. Flow rates for the two loads are listed in Table 1. The size distribution after primary fragmentation shown in Table 2 was used as an input to the simulation. The characteristics of the local high ash coal are also listed in Table 2. The heating value of the fuel is 7.7 MJ/kg (a.r.). The total coal feed rate was in the simulation adjusted to satisfy the oxygen balance based on the measured O_2 concentration in the backpass. At the higher 120 MWe load, significantly larger amounts of fuel and secondary air were fed to the left half of the furnace, while at the lower 80 MWe load the division was more even. At both loads the amount of primary air was fairly small, so that the superficial gas velocity at bed bottom remained below 2 m/s.

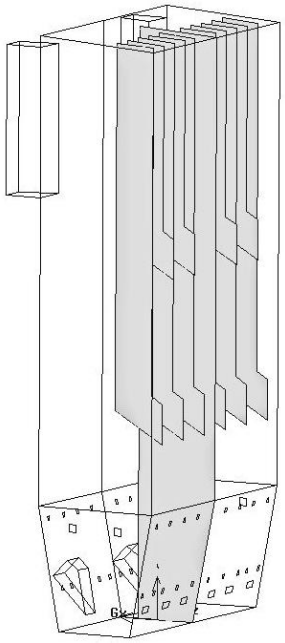

Figure 1. Boiler geometry.

Table 1. Air and fuel flow rates at loads 120 MWe and 80 MWe.

High load 120 MWe									
Air flow	**Primary**	**To coal feeders**	**To ash coolers**	**To loop seal**		**Upper secondary**		**Lower secondary**	
				Left	**Right**	**Left**	**Right**	**Left**	**Right**
kg/s	46.5	4.7	10.7	0.34	0.35	21.7	9.2	19.1	11.0

Fuel flow	**Feeder 1**	**Feeder 2**	**Feeder 3**	**Feeder 4**	**Feeder 5**	**Feeder 6**
kg/s	6.3	7.9	8.1	7.9	4.0	3.0

Low load 80 MWe									
Air flow	**Primary**	**To coal feeders**	**To ash coolers**	**To loop seal**		**Upper secondary**		**Lower secondary**	
				Left	**Right**	**Left**	**Right**	**Left**	**Right**
kg/s	38.2	4.3	11.3	0.37	0.36	14.8	14.9	8.2	10.3

Fuel flow	**Feeder 1**	**Feeder 2**	**Feeder 3**	**Feeder 4**	**Feeder 5**	**Feeder 6**
kg/s	1.4	5.7	3.9	6.7	3.1	1.2

Table 2. Particle size distribution of coal after primary fragmentation and coal analysis results.

Size, mm	**0.0 - 0.5**	**0.5 – 1.0**	**1.0 – 2.0**	**2.0 - 3.2**	**3.2 – 6.0**	**> 6.0**
%	31.2	16.2	26.3	11.1	8.5	6.7

Volatiles [wt% daf]	**Proximate [wt% a.r.]**			**Ultimate [wt% daf]**				
	Comb.	**Ash**	**Moist.**	**C**	**H**	**O**	**S**	**N**
41.7	32.6	62.6	4.8	56.9	7.7	32.1	1.8	1.6

Pressure and temperature profiles, flue gas composition and heat exchanger data were collected during the experiments. Additional measurements of temperature, gas composition and particle size distribution were carried out at four distances from the wall through four measurement ports on the right side wall of the furnace at 17.9 m and 27.4 m heights, and in the cyclone inlet channel at 30.6 m height. Particle size was

determined even from a bottom ash sample. The measurements were carried out in between normal power plant operation.

3 Modeling

3.1 Model for hydrodynamics

A steady-state CFD modeling approach based on time-averaged Eulerian-Eulerian equations for hydrodynamics of a gas-solid suspension was introduced in Taivassalo *et al.* (2011). By ignoring density fluctuations, the time-averaged continuity and momentum equations can be summarized for a phase q as follows

$$\nabla \cdot \overline{\rho}_q \overline{\alpha}_q \mathbf{U}_q = 0 \tag{1}$$

$$\begin{aligned} \nabla \cdot \overline{\alpha}_q \overline{\rho}_q \mathbf{U}_q \mathbf{U}_q = {} & \overline{\alpha}_q \overline{\rho}_q \mathbf{g} - \overline{\alpha}_q \nabla \overline{p} - \overline{\alpha'_q \nabla p'} + \nabla \cdot \overline{\alpha_q \boldsymbol{\tau}_q} + \nabla \cdot \overline{\alpha_q \boldsymbol{\tau}^M{}_q} \\ & + (-1)^{(\delta_{qs}+1)} \overline{K_{gs}\left(\mathbf{u}_g - \mathbf{u}_s\right)} - \delta_{qs} \nabla \overline{p}_s - \nabla \cdot \overline{\rho}_q \overline{\alpha_q \mathbf{u}''_q \mathbf{u}''_q} \end{aligned} \tag{2}$$

Here ρ is the density, α volume fraction, p pressure, p_s solid pressure, $\mathbf{g}$ gravitational acceleration, K inter-phase momentum transfer coefficient, δ_{gs} Kronecker delta, $\boldsymbol{\tau}$ laminar stress, and $\boldsymbol{\tau}^M$ local-scale turbulent stress. The time average of a variable φ is denoted by $\bar{\varphi}$ and the fluctuation part by $\varphi' = \varphi - \bar{\varphi}$. In the equations above, $\mathbf{u}$ is the instantaneous velocity, $\mathbf{U}_q$ is the Favre average or phase-weighted average velocity $\mathbf{U_q} = \overline{\alpha_q \mathbf{u_q}}/\overline{\alpha_q}$ and $\mathbf{u}''_q = \mathbf{u}_q - \mathbf{U}_q$ is the velocity fluctuation. The gas phase is denoted by g and solid phase by s. The terms on the right hand side in Equation (2) are, from left to right, the gravitation, pressure, pressure fluctuation, laminar stress, turbulent stress, drag force, solid pressure, and Reynolds stress terms. The gravitation and pressure terms can be directly calculated from the time-averaged flow properties but for the rest of the terms closure relations need to be applied. In Taivassalo et al. (2011), closure relations were derived on the basis of data from transient simulations that were to a good extent validated by comparisons with measurements. Peltola et al. (2013) modified the closures to include solution of all Reynolds stress components for the solid phase from balance equations. The other terms are modeled through algebraic correlations. In the description of mixing in the gas and solid phases, correlations for the time scales of the velocity fluctuations based on the results of Peltola & Kallio (2012) are employed.

3.2 Modeling of heat transfer and chemistry

In the time-averaged transport equation for a gas-phase species, the velocity fluctuations (Reynolds stresses) and their time scales are used to estimate a local value for an isotropic dispersion coefficient needed in the calculation of the dispersion flux. The gas phase is described (Taivassalo et al. (2012)) as a mixture of seven species, O_2, N_2, CO_2, CO, H_2O, H_2 and a general volatilized gas CH_xO_y. The complex gas-phase chemistry is modeled by net oxidation reactions of CH_xO_y, CO and H_2. The time-averaged reaction rates are assumed to be limited by gas-phase mixing.

The Lagrangian particle tracking approach is employed for the fuel. The solid-phase average velocity field, velocity fluctuations and time scales are used in determining the

instantaneous velocity components for the tracked particle. For the drag force between the fuel particles and the Eulerian solid phase, the model of Syamlal (1987) is applied and for gas particle drag the same correlation that is used for the bed material. Large fuel particles leaving the furnace that are assumed to be separated by the cyclone are returned to the furnace with the solid bed material. Evaporation, devolatilization, combustion and gasification of the fuel particles are modelled with the approach presented by Taivassalo et al. (2012).

The magnitude and time scales of the velocity fluctuations are used to predict a representative value for the isotropic heat transfer coefficient. In the calculation of the heat exchange coefficient h_{sg}, the model of Gunn (1978) is used for the Nusselt number. The heat transfer coefficient between the gas-solid suspension and the walls is computed from the model of Nirmal Vijay and Reddy (2005). In addition, in the current case the simplest radiation model, the P1 model, of Fluent was activated and the solids volume fraction was used to evaluate the dispersion and scattering coefficient. In typical CFB conditions, the range of visibility is so short that even the P1 model, suitable for optically thick media (Ansys, (2012)), is considered satisfactory.

3.3 Simulation method

The Ansys Fluent 14.5 (Ansys (2012)) code was used to obtain a steady-state solution of the coupled transport equations and to carry out the tracking of representative fuel particles. The computational mesh consisted of approximately 2 million elements.

To approximate the distribution of particles of different sizes in the furnace, the particle diameter was set as a function of riser height. At the bottom the size was set at 0.45 mm on basis of an analysis of bottom ash samples and at the top at the median size in the samples taken at 17.9 m height.

The bed mass was estimated from the measured pressure profile. Outlet boundary pressures are set the same for both outlets, because the pressure measurement provided by the automation system for the left outlet was not credible.

The Lagrangian description of the fuel particles proved very time consuming in such a large boiler. The fuel particles spend considerable time in the boiler, requiring a large number of time steps to be calculated for each particle. As the results affect the Eulerian flow solution, a large number of iterations between the Eulerian and Lagrangian results should be carried out. The number of iterations done in this work was not necessarily large enough to guarantee fully converged results, but sufficient for the present analysis.

4 Results

At the higher load, the higher air and fuel mass flows in the left half of the furnace produce asymmetric results as seen in the velocities and in the net heat of reactions (per computational cell) in Figure 2. Generally there is a falling wall layer of solids on all the walls and heat exchangers. The secondary air tends to locally form a high velocity vertical channel all the way to the outlet. There is significant variation in the wall layer thickness in different locations, but since no velocity profile data is available from the furnace, there is significant uncertainty in the assessment of the correctness of the

results. The distributions obtained at the lower load, shown in Figure 3, are more uniform on the two sides of the furnace as could be expected on basis of the inlet flow rates given in Table 1. Combustion takes place at a lower level at the lower load.

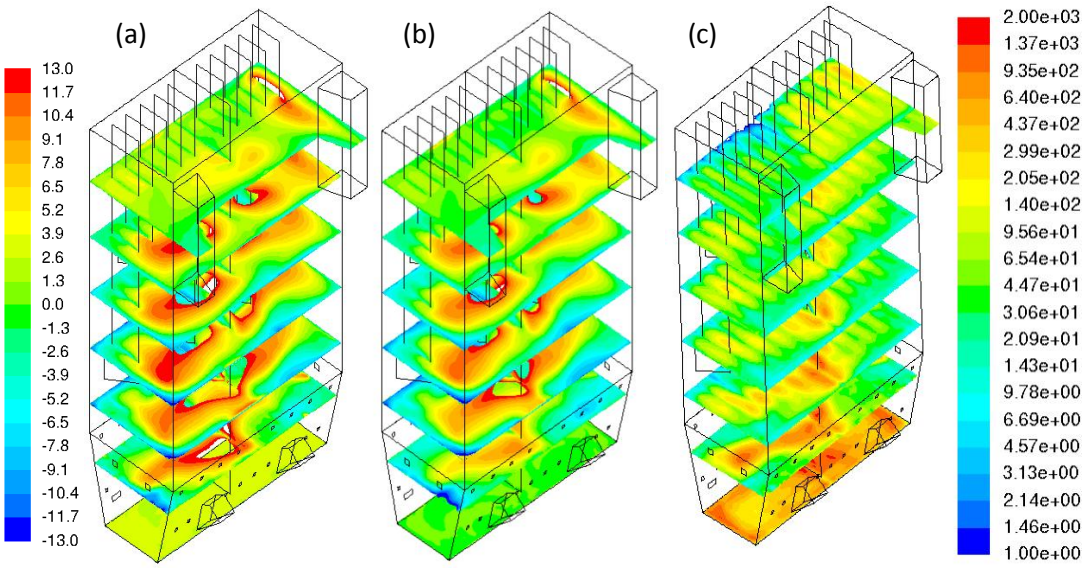

Figure 2. Contours of simulated gas (a) and solids (b) vertical velocities [m/s] and (c) net heat of reaction [W/cell] at 120 MWe load.

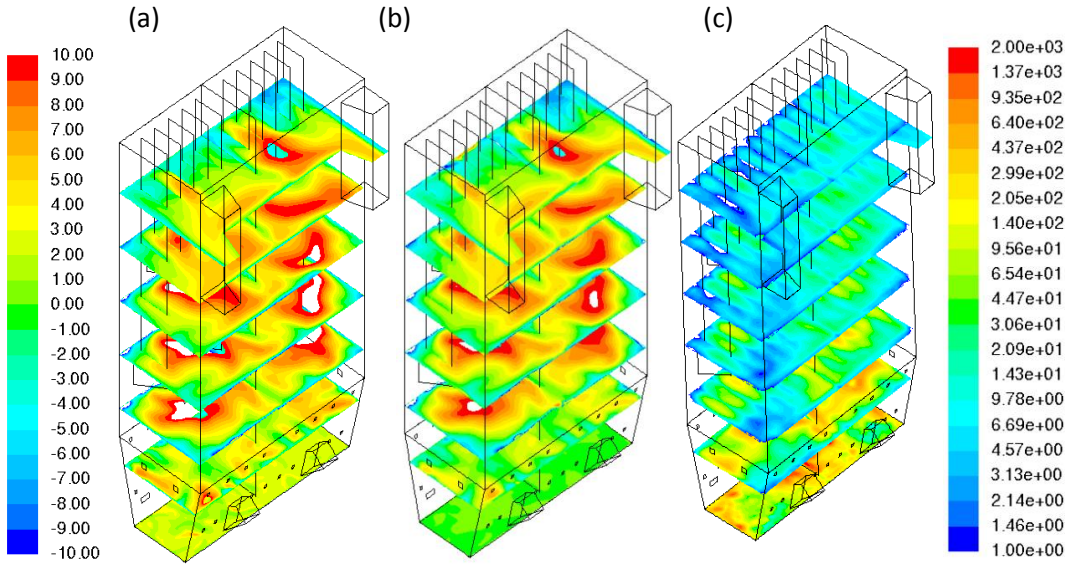

Figure 3. Contours of simulated gas (a) and solids (b) vertical velocities [m/s] and (c) net heat of reactions [W/cell] at 80 MWe load.

Similar difference in asymmetry as between Figures 2 and 3 can be seen in the volume fraction contours of Figure 4. At the lower load, the bed mass is concentrated in the region below secondary air inlets while at the higher load the solids concentration is higher up to riser top, resulting in a significantly higher solids recirculation rate.

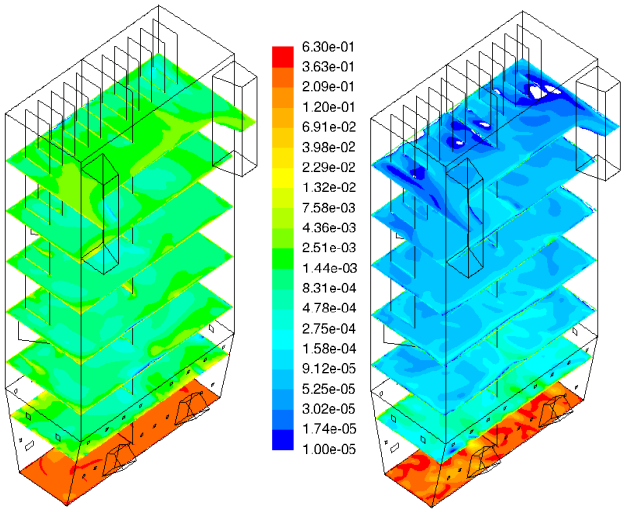

Figure 4. Solids volume fraction contour at 120 MWe (left) and 80 MWe loads.

Figure 5 shows a comparison of measured O_2 and CO concentrations to selected vertical profiles from the simulation at 120 MWe load and the simulated profiles at 80 MWe load. The measurement locations do not coincide exactly with the sampling lines of the simulation in all locations. The simulated profiles are somewhat uneven, showing local variations in the temperature and species concentrations. This may be a symptom of inadequate number of Lagrangian fuel particles.

The vertical oxygen concentration profiles show, as expected, a region of low oxygen below the secondary air level. At the lower load the low O_2 region is more distinct. This is in agreement with the plot of heat of reactions in Figure 3, which shows that the fuel mainly burns in the bottom section at the lower load.

At the measurement location near the walls the simulated oxygen concentrations are higher than measured. This is probably an indication that the vertical channel formed by the secondary air jet at this wall in the simulation may not be as strong in the real boiler. There is a lot of variation in the vertical CO profiles, but if any conclusion can be drawn, at the measurement locations the results are in similar range. At both loads, CO concentration is high in the region below the secondary air inlet level.

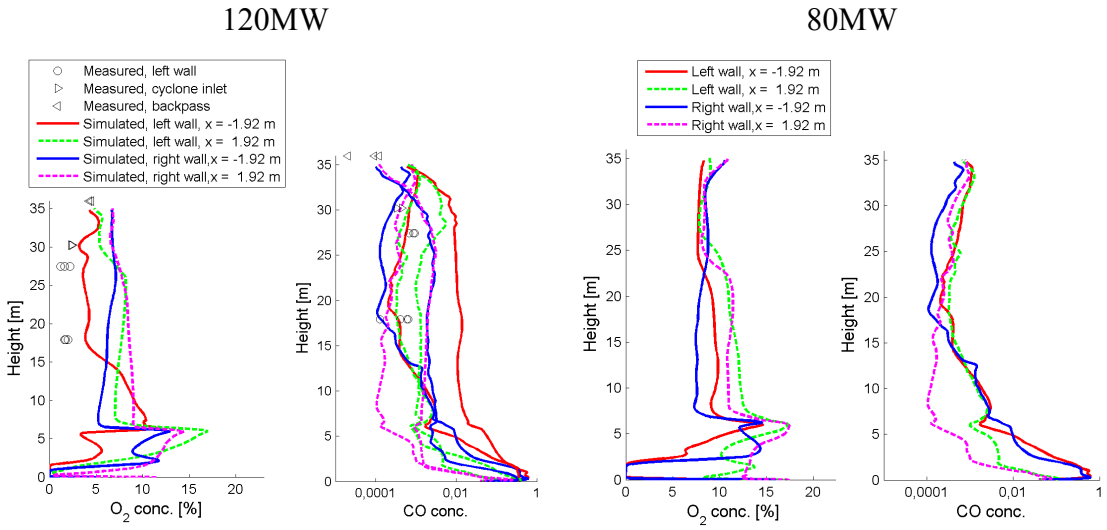

Figure 5. Comparison of simulated vertical O_2 and CO concentration profiles to measured values at 120 MWe load and the simulated profiles at 80 MWe load.

A comparison of measured and simulated temperatures near the walls at 120 MWe load is shown in Figure 6, in addition to the simulated profiles at 80 MWe load. At 120 MWe load, highest temperatures have been measured at 17.9 m height, but the simulated temperatures are generally lower than measured. Temperatures are in general lower at the lower load.

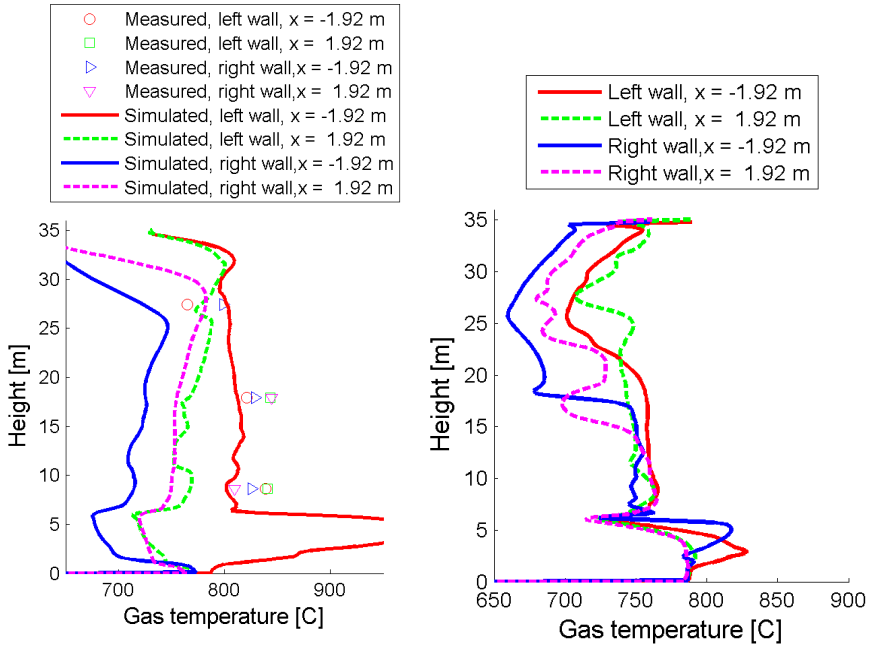

Figure 6. Comparison of simulated vertical gas temperature profiles to measured values at 120 MWe load (left) and corresponding simulated profiles at 80 MWe load (right) in the vicinity of the side walls.

5 Conclusions

A steady-state simulation approach was applied to a 135 MWe circulating fluidized bed combustor at two loads to examine its capabilities in a commercial scale CFB. The results were presented and compared at the higher load with measurement data from a measurement campaign carried out at the power plant. Temperature and gas composition data were compared with measurements.

While the Eulerian time-averaged simulation is quite fast, iterating the Eulerian solution and the Lagrangian simulation of the fuel particles proved very time consuming in a large boiler. There is a possibility for some improvement by optimizing the Lagrangian particle code, but it is likely that, if a Lagrangian fuel description is used, the Lagrangian portion of the simulation will remain the limiting factor for simulation speed. Thus shifting to Eulerian fuel description should be considered in the future.

The simulation results show the typical characteristics of a CFB, i.e. a dense suspension region at the furnace bottom and more dilute conditions higher up. Dense, falling layers of solids are found on the walls and heat exchangers. The asymmetric fuel and air inlets at the higher load produced an asymmetric flow field also in the simulation.

Gas composition profiles show local variation, possibly due to an inadequate number of Lagrangian fuel particles. Simulated oxygen concentration at the near-wall measurement locations is higher than measured, indicating that the near-wall channelling effect of the secondary air may be somewhat over predicted in the simulation. The low oxygen concentration region below the secondary air feed level, which is typical of staged combustion, is well produced by the simulations.

The observed probable discrepancies to reality can be a consequence of a fixed vertical mean particle diameter profile and of the limited amount of data used as basis for the derivation of equation closures for the time-averaged balance equations. These shortcomings are addressed in the research efforts made presently by the authors and thus even better results are expected in the future.

6 Acknowledgements

The authors gratefully acknowledge the financial support of Tekes, VTT Technical Research Centre of Finland, Etelä-Savon Energia Oy, Fortum, Metso Power Oy and Numerola Oy, and the support from Saarijärven Kaukolämpö Oy. The invaluable contribution of the power plant personnel and the assistance of all the people participating in the experiments, especially Prof. Yang at Tsinghua University, are gratefully acknowledged.

LIST OF SYMBOLS

g	gravitational acceleration	$[m^2/s]$
K	drag coefficient	$[kg/m^3s]$

p	pressure	[Pa]
u	velocity	[m/s]
x	spatial coordinate	[m]
α	volume fraction	[ ]
δ_{ij}	Kronecker delta	[ ]
ρ	density	[kg/m^3]
σ	standard deviation	
τ	stress	[kg/m s^2]

REFERENCES

Andrews, M.J. and O'Rourke, P.J. 2011. The Multiphase Particle-in-Cell (MP-PIC) Method for Dense Particle Flows. Int. J. of Multiphase Flow, 22(2):379–402.

Ansys inc. 2012. Ansys FLUENT theory guide, Release 14.5.

Benyahia, S., Sundaresan, S. 2012. Do we need sub-grid scale corrections for both continuum and discrete gas-particle flow models? Powder Technology, 220, pp. 2 - 6

Gunn, D.J. 1978. Transfer of heat or mass to particles in fixed and fluidized beds, Int. J. Heat Mass Transfer, Vol 21, pp. 467-476 (in Ansys Inc., 2012).

Nikolopoulos A., Rampidis I., Nikolopoulos N., Grammelis P., Kakaras, E. 2010. Numerical investigation of 3-D transient combusting flow in a 1.2MWth pilot power plant, Proceedings of the 20th Int. Conf. on FBC, pp. 839–844.

Nirmal Vijay, G., Reddy, B.V. 2005. Effect of dilute and dense phase operating conditions on bed-to-wall heat transfer mechanism in a circulating fluidized combustor. Int. J. Heat and Mass Transfer Vol. 48, pp. 3276-3283.

Pallarès, D., Johnsson, F. 2006. Macroscopic modelling of fluid dynamics in large-scale circulating fluidized beds. Progr. in Energy and Combustion Science, 32, pp. 539 – 569.

Peltola, J., Kallio, S. 2012. Estimation of turbulent diffusion coefficients in a CFB on basis of transient CFD simulations, FBC21, Naples, Italy.

Peltola, J., Kallio, S., Yang, H., Qiu, X, Li, J. 2013. Time- averaged simulation of the furnace of a commercial CFB boiler, accepted to Fluidization XIV, Noordwijkerhout, The Netherlands.

Syamlal, M. 1987. The particle-particle drag term in a multiparticle model of fluidization. National Technical Information Service, Springfield, VA, USA. DOE/MC/21353-2373,NTIS/DE87006500 1987 (referenced in Ansys Inc., 2012).

Taivassalo, V., Kallio, S., Peltola, J. 2011. On time-averaged CFD modeling of circulating fluidized beds, 12th Int. Conf. Multi-Phase Flow in Industrial Plants, Ischia, Italy.

Taivassalo, V., Peltola, J., Kallio, S. 2012. Time-averaged CFD modeling of a circulating fluidized bed combustor, FBC21, Naples, Italy.

Zhang, N., Lu, B., Wang, W., Li, J. 2010. 3D CFD simulation of hydrodynamics of a 150 MWe circulating fluidized bed boiler, Chem. Eng. Journal, 162, pp. 821–828.